

Flexoelectrically Driven Instabilities in Liquid Crystals

K. S. Krishnamurthy, Pramoda Kumar AND Pramod Tadapatri

Abstract | Flexoelectricity is an important mechanoelectric property of liquid crystals that provides a reciprocal, linear relation between curvature distortions and electric polarization. We review here a few of the less known electric field generated flexoelectric effects observed in recent years and relating to (a) dc field excited flexo-response at defect sites in nematic inversion walls, (b) gradient flexoelectric switching at polarity reversals in nematics, (c) flexoelectrically driven phase propagation in the undulatory structure of the smectic C phase and (d) asymmetric distortion in sheared annular walls in free-standing nematic films.

1. Introduction

Flexoelectricity in liquid crystals (LCs), predicted very early by Meyer¹, is a mechanoelectrical phenomenon analogous to piezoelectricity in solids. But unlike the latter, which arises from translational deformations and requires the material to be non-centrosymmetric, the former is generated by curvature strains in LCs regardless of their symmetry². This aspect is readily appreciated in uniaxial nematics which possess a long-range orientational order but no translational order; their direction of axial symmetry is given by a unit vector \mathbf{n} , called the *director*. A strain-free nematic is centrosymmetric being invariant with respect to $\mathbf{n} \rightarrow -\mathbf{n}$ operation and any rotation about \mathbf{n} . Curvature deformations of the splay and bend type break this symmetry and enable a non-vanishing local polarization to develop in the medium. Following the Meyer sign convention¹, the polarization density \mathbf{P} so induced may be written as

$$\mathbf{P} = e_S \mathbf{n}(\nabla \cdot \mathbf{n}) + e_B (\nabla \times \mathbf{n}) \times \mathbf{n} \quad (1)$$

where e_S and e_B are the flexoelectric (or 'flexo-' for short) coefficients appropriate to the splay and bend distortions, respectively. Flexocoefficients

are experimentally found to be of the order of $10^{-11} \text{ C m}^{-1}$ in many rod-like (calamitic) systems; interestingly, as recent findings show, in bent-core nematics, e_B could be $\sim 10^3$ times greater³.

From a microscopic view-point, flexopolarization may arise from a coupling between molecular shape polarity and permanent dipolar moments as schematically illustrated in Figure 1¹. Even in more symmetric mesogenic molecules, flexoeffect is possible through the electric quadrupole mechanism first proposed by Prost and Marcerou⁴. A gradient in quadrupole density brought about by a splay or bend distortion could generate a bulk polarization as depicted in Figure 2⁴.

Analogous to the converse piezoelectric effect in solids, there exists the inverse or converse flexoeffect in LCs in which an applied electric field causes curvature distortions in the fluid so as to produce a net polarization along the applied field and thereby reduce the free energy. Evidently, in various electric field induced phenomena in LCs, flexopolarization plays a discernable role. Apart from its technological importance such as seen in zenithal bistable displays^{5a} and post-aligned bistable nematics^{5b}, flexoelectricity is also of fundamental interest because of its near universal presence in LCs exposed to electric fields. For

Carr-Helfrich: Carr-Helfrich mechanism refers to the coupling between electrical conductivity anisotropy and bend curvature distortion in a nematic under the action of an electric field; it results in the formation of periodic space charges.

Homogeneous alignment: Homogeneous alignment implies the orientation of the nematic director parallel to the substrates, along a common direction.

Figure 1: The Meyer dipolar model of flexoelectricity in nematics formed of molecules with shape polarity and permanent dipole moment¹. (a) Nonpolar order of wedge-shaped molecules with a longitudinal moment (blue-red arrow) in the absence of strain; (b) splay distortion producing a net local polarization P for $e_s > 0$. (c) Non polar order of crescent-shaped molecules with a transverse moment in the strain-free state; (b) bend-distortion producing a net polarization P for $e_b > 0$.

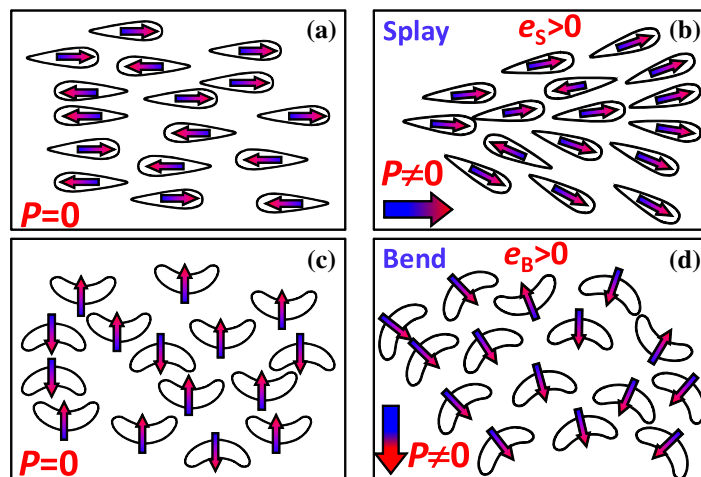
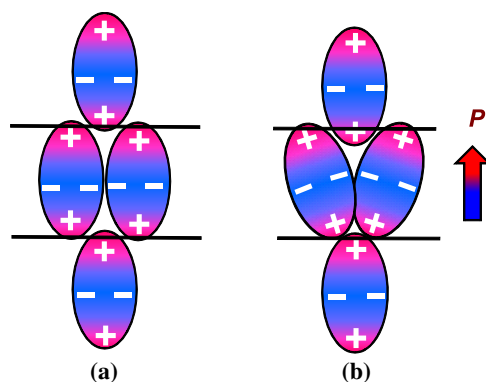


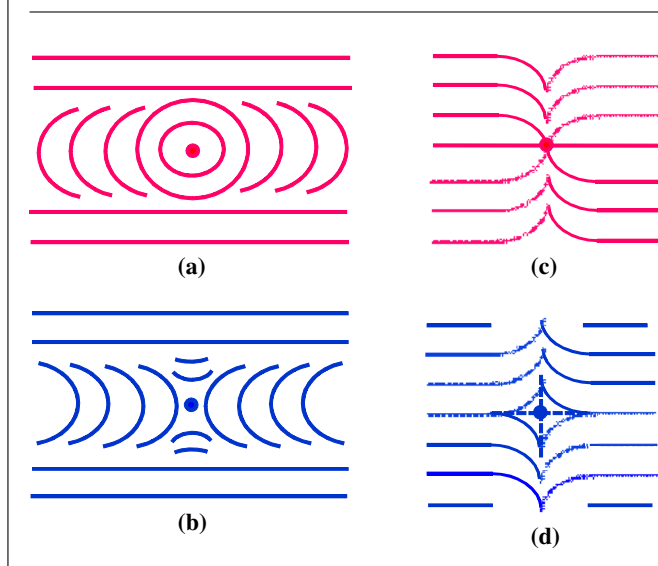
Figure 2: The Prost-Marceau quadrupolar model of flexoelectricity in liquid crystals formed of symmetric nonpolar molecules³. (a) Quadrupolar assembly in the distortion-free state with no bulk polarization. (b) Splay distortion causing asymmetry in charge distribution: The positive charges from the top and bottom layers move respectively toward and away from the mid-layer, resulting in a net dipole moment.



example, electroconvective pattern characteristics in planar nematics are known to be modified by flexoelectricity; by inclusion of flexoterms in the Carr-Helfrich mechanism based theories⁶, it has been possible to account for the threshold oblique-rolls occurring below a critical frequency in usual nematics with the conductivity anisotropy ($\sigma_a = \sigma_{||} - \sigma_{\perp}$, $||$ and \perp denoting the directions relative to the director) being positive, and the longitudinal rolls in nematics with $\sigma_a < 0$. However, these and other *well known* results that establish the

relevance of flexoelectricity to electrohydrodynamic structures in calamitic nematics are not the subject of this article. Our purpose here is to review some of the *less known* flexo-related electric field effects in LCs observed in recent years⁷⁻¹⁰. They pertain to (a) dc field switching at nematic defect sites, (b) gradient flexoelectric analog of the Freedericksz effect (dielectric reorientation) in nematics, (c) propagating undulations in the smectic C phase and (d) asymmetric distortion in sheared annular walls in free-standing nematic films.

Figure 3: Defects in nematic inversion walls¹¹. (a) +1 tangential defect in a wall parallel to the easy axis. (b) -1 defect in a wall parallel to the easy axis. (c) +1 radial defect in a wall normal to the easy axis. (d) -1 defect in a wall normal to the easy axis.



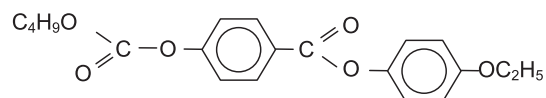
2. Flexoresponse at ± 1 defect sites in nematic π -walls

2.1. Inversion walls

The homogeneous alignment of a nematic film sandwiched between unidirectionally buffed transparent electrodes, such as indium tin oxide (ITO) coated glass plates, is often imperfect due to the formation of several narrow vertical walls that bridge regions of parallel and antiparallel alignments; within these so-called *inversion walls*, the director progressively rotates through an angle π . The walls parallel to the easy axis or director are of the bend type and those normal to it, of the splay type. Walls of opposite bend or splay are connected by line defects¹¹. In Figure 3 illustrating these features, the line singularities are the so-called wedge disclinations of unit strength. While these disclinations could exist in the bulk, the walls are expected, from energy considerations, to be stable only at the substrates where a definite orientation is imposed and to smear out in the bulk¹². Experimentally, however, it is often found that, in freshly prepared thin nematic samples, even the inversion walls remain stable for long periods of the order of days⁷.

The curvature distortions associated with the defect structures lead to flexoelectric charge separation. Thus, the wedge disclinations in Figure 3 are all electrically charged; assuming the flexocoefficients to be positive, the core is positive for the +1 defect in Figure 3a and negative for the remaining defects in Figures 3b–d. However, in the absence of an external electric field, for

symmetry reasons, there may be no net polarization. Application of the field could disturb the symmetry by distortion of the director configuration and generate a net polarization along the field. We may now review a recent demonstration of this result in butyl p-(p-ethoxyphenoxy) carbonyl phenyl carbonate (BEPC) with the following chemical structure; it occurs in the nematic state between ~ 55 and 84°C ⁷.



2.2. Switching at a +1 defect

Figure 4 shows a +1 defect formed in a bend inversion wall parallel to the easy axis x , as observed for P(45)–A(135), where P denotes the polarizer, A the analyzer and the numbers in parentheses denote the angles made by the transmission axes with x . Immediately around the defect centre, the birefringence colour is first order white while farther off it has risen to the brown of the same order corresponding to a change in retardation by about 250 nm. This indicates that the defect-core is rendered nonsingular in bulk through the so-called director escape. The escaped configuration (Figure 5) is obtained by incorporating a progressive director twist along any radius in the configuration in Figure 3a, so that only surface singularities remain. Upon application of a static field the following effects are observed: The extinction cross at a given

Figure 4: Texture of a +1 line defect in an inversion wall formed parallel to the easy axis \mathbf{n} in a 4.6 μm thick nematic film of BEPC at 70°C. The polarizer P and analyzer A are diagonally crossed. E denotes the electric field. Applied voltage is +5 V in (a), 0 in (b) and -5 V in (c). Horizontal dimension is 50 μm . (From ref.7).

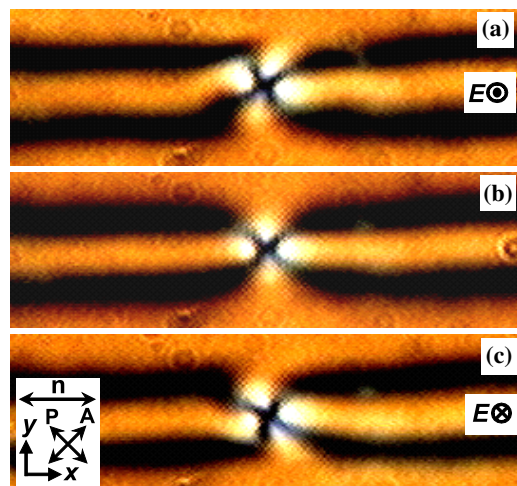
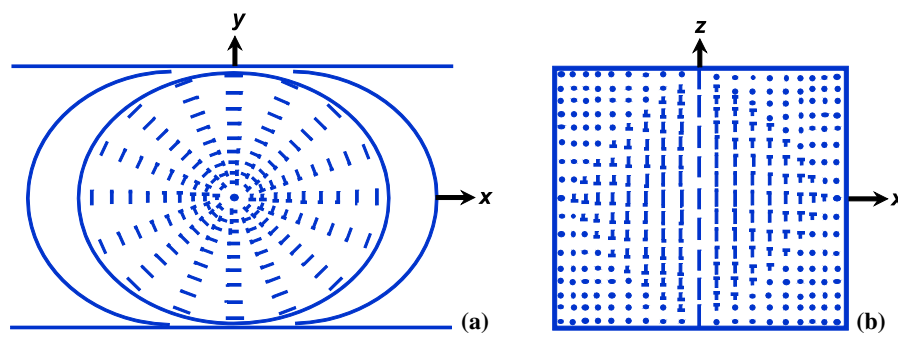


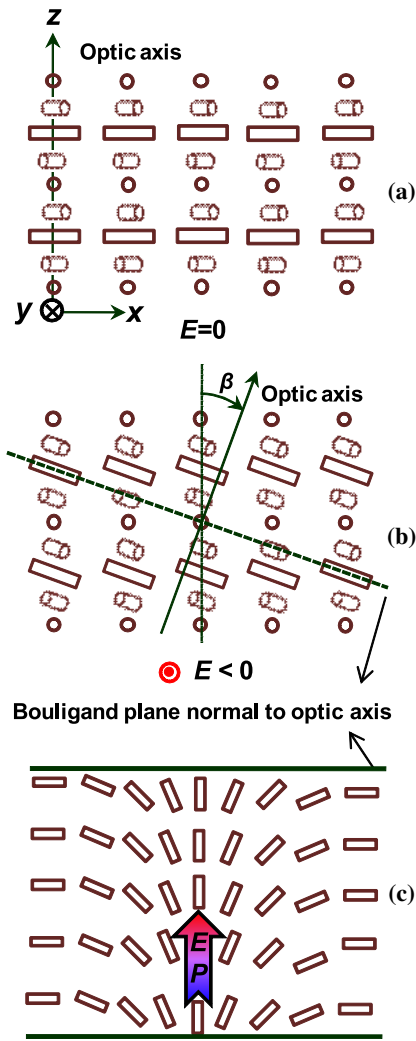
Figure 5: The director field at a +1 defect site. (a) Midplane $z=0$. (b) Vertical section $y=0$. Nails signify out-of-plane tilts of the director. (From ref.7).



defect site rotates either clockwise or anticlockwise; the sense of rotation reverses on reversal of the field direction (Figures 4a, 4c). For a given field direction, the rotational sense at different +1 sites varies in general. With a low frequency ac field, the switching effect is detectable down to a fraction of a volt. Most importantly, the degree of rotation changes linearly with field strength; this points to the flexoelectric origin of the switching effect. These observations are reminiscent of the electro-optic effects found by Rudquist *et al.*¹³ in twisted bipolar nematic droplets formed of achiral molecules. While in such droplets the director twist occurs about both horizontal and vertical directions, in a +1 defect the twist is only about the radius and the substrate planar alignments are reached primarily

through splay bend distortions (Figure 5b). Despite this structural difference, the basic mechanism of field driven deformation in both cases is the flexoelectrooptic (FEO) effect which was discovered by Patel and Meyer in the course of their electrooptic experiments on cholesterics¹⁴. Figure 6 illustrates the FEO effect with reference to the helical structure of cholesterics. When a static electric field is applied transverse to the helix axis, the local director rotates about the field direction thereby turning the optical axis through an angle $\beta = \tan^{-1}[eEp/(2\pi k)]$. Here k is the average of splay (k_{11}) and bend (k_{33}) elastic constants, p the helix pitch, E the applied field and e the average flexocoefficient $(e_S + e_B)/2$. In any plane transverse to the new optical axis, a periodic splay bend curvature develops in a way that a net

Figure 6: Flexoelectrooptic effect in chiral nematics. (a) Field free state. (b) Field E applied transverse to the helix axis, along $-y$, induces a rotation of the local director through an angle β . (c) Splay-bend distortion in the Bouligand plane normal to the optic axis leading to flexopolarization P along E .



flexoelectric polarization is generated along the field direction (Figure 6c).

Now consider a +1 disclination along z , with the director confined to the xy plane; the director tilt φ with respect to x in a plane transverse to z is then expressible as¹¹ $\varphi = \tan^{-1}(y/x) + \alpha$ where α is a constant angle denoting the director deviation at any point from the radius through that point. Thus, in general, the flux lines are logarithmic spirals; the director field is purely radial for $\alpha = n\pi$, n being an integer; and it is circular, for $\alpha = n\pi/2$. For the escaped configuration of a +1 defect (Figure 5), $\alpha = \pi/2$ at the substrates; in the bulk, there exists an added director twist about the radial direction. Application of a small dc field alters α slightly, say by

β ($\ll \pi/2$); then the midplane director projections delineate logarithmic spirals (Figure 7). Now in a vertical plane through any spiral field line, the director will have a splay bend pattern similar to that in Figure 6c such that the resulting flexoelectric polarization is along the field. The sign of β , for a given e and E , is determined by the sign of helix wave vector. Since the latter has equal probability of being positive or negative, the clockwise and anticlockwise switchings occur with equal probability among the +1 defects in walls parallel to the easy axis.

The switching at -1 defect sites is more complex than that at +1 sites and involves both radial and tangential c-director fields; however, it is possible to interpret this switching through the converse flexo and FEO effects.

3. Gradient flexoelectric switching in nematic BEPC exposed to low frequency fields

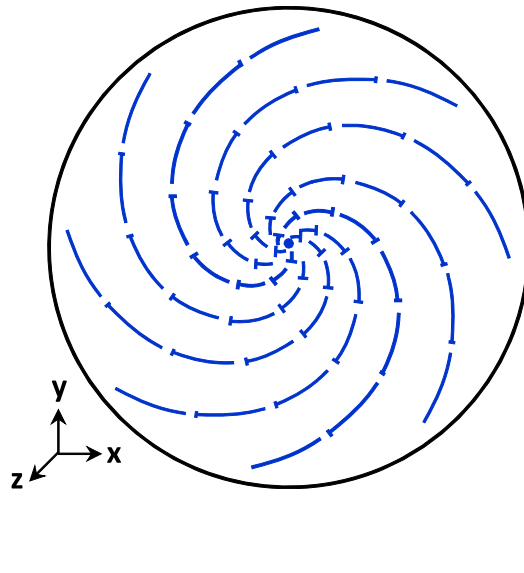
The bulk flexotorque causing field-induced deformation is expressible as $\mathbf{n} \times \mathbf{h}$, \mathbf{h} being the molecular field given by¹⁵

$$\mathbf{h} = (e_S - e_B)(\mathbf{E}\nabla \cdot \mathbf{n} - \nabla \mathbf{n} \cdot \mathbf{E}) - (e_S + e_B)\mathbf{n} \cdot \nabla \mathbf{E} \quad (2)$$

Here the first term on the right hand side applies to the flexoeffect induced by a uniform electric field; the second term is associated with the so called gradient flexoelectric (GF) effect caused by an inhomogeneous field¹⁵⁻¹⁷. An example of the homogeneous field volume effect is the Bobylev and Pikin^{16,18} (BP) instability appearing above a voltage threshold V_f in nematics with strong planar anchoring and $|\epsilon_a| < (e_S - e_B)^2/k$, the elastic constant k denoting k_{11} (splay) = k_{22} (twist). Optically, it appears as periodic domains with the wave vector q along y (transverse to \mathbf{n} ; the corresponding director pattern is given by $\Theta = \Theta_o \cos(qy) \cos(\pi z/d)$ and $\Phi = \Phi_o \sin(qy) \cos(\pi z/d)$, where Θ and Φ represent the director tilts from x in the xz and xy planes, respectively. Besides this (Θ, Φ) instability, as we shall describe presently, BEPC also exhibits a novel transient switching response that may be interpreted as the GF effect due to the second term in eq. (2).

Although the initial planar alignment of BEPC remains undisturbed in a steady field of voltage amplitude less than V_f , before the steady conditions set in after the field is turned on, a momentary change of molecular alignment takes place. This transient phenomenon is best appreciated using a very low frequency square wave field instead of dc, and monitoring the intensity transmitted by the sample kept between diagonally crossed polarizers. Figure 8 illustrates a typical electrooptic response

Figure 7: Logarithmic spirals defined by director projections in $z=0$ plane. Splay-bend arc pattern of alignment is present in any vertical plane (Bouligand plane) containing opposite spiral arms. This configuration is for E along z , $e > 0$ and an initially right handed helical structure ($k > 0$), as in figure 5. (From ref.7).



in such a situation for a sample subject to a 5 mHz square wave field; here, the brief changes in intensity that follow each polarity reversal are indicative of the occurrence of transient director switching at twice the frequency of the applied field. Evidently, the switching mechanism is related to the electric field inhomogeneity that may be expected to exist in bulk during the counterion transport. In the steady state, between switchings, when the field becomes uniform in bulk and the gradients are confined to the immediate vicinity of the electrodes, no detectable intensity change occurs.

Optically, with the sample held between diagonally crossed polarizers, the interference colour on Newton's scale downshifts during the buildup of distortion and then the initial state is reestablished. For example, in the unperturbed state, the birefringence colour of the sample with which the profile in Figure 8 is recorded, is green of the second order (Figure 9a). Figures 9b–9d showing some of the textures captured during the switching process indicate the nature of structural change. At lower voltages, the sample displays a uniform colour as in Figures 9b and 9c, suggesting the distorted state to be homogeneous and analogous to the usual Freedericksz state. At higher voltages, the perturbation evolves into a patterned state; Figure 9d shows the texture obtained in the early part of this evolution.

We may invoke the GF effect to interpret the homogeneous and periodic instabilities just

described. It has been shown that, under certain conditions, a planar nematic can display a GF *volume* instability reminiscent of the splay-Freedericksz distortion^{17b}. For example, assuming dielectric isotropy [$\varepsilon_a = (\varepsilon_{||} - \varepsilon_{\perp}) = 0$], elastic isotropy ($k_{11} = k_{22} = k_{33} = k_i$) and a linear decrease in the field from E_a at the anode to E_c at the cathode, the balance between the elastic and GF torques yields the instability threshold V_G ^{17b}

$$V_G = \frac{\pi^2}{2} \left(\frac{E_a + E_c}{E_a - E_c} \right) \frac{k_i}{e^*}; \quad e^* = e_S + e_B. \quad (3)$$

From the known range of variation of k_i/e^* (0.2 to 1 Nm/C)¹⁵, and taking $E_a = 10E_c$ for argument, we estimate V_G to be of the order of a few volts.

When $\varepsilon_a > 0$, the planar sample is dielectrically unstable; then, besides the GF torque Γ_G , the Freedericksz torque Γ_F enters the torque balance equation. Under a low voltage and a large field gradient, however, only Γ_G will be prominent. For example, when the distortion is homogeneous splay under a constant field gradient,

$$\frac{\Gamma_G}{\Gamma_F} = \frac{e^* \sin\theta \cos\theta (dE/dz)}{\varepsilon_o \varepsilon_a \sin\theta \cos\theta E^2} = \frac{e^*}{\varepsilon_o \varepsilon_a V} \left(\frac{E_a - E_c}{E_a + E_c} \right) \quad (4)$$

Using $e^* \sim 10^{-11}$ C/m, $\varepsilon_a = 0.1$, $V = 1$ V and $E_a/E_c = 10$, we obtain $\Gamma_G \approx 9\Gamma_F$. The switching in BEPC at low voltage amplitudes may therefore be regarded as essentially a GF response.

Figure 8: Transient switching in a $7.75 \mu\text{m}$ thick layer of BEPC. Parallel polarizers, P(45)-A(45). 5 mHz square wave excitation. Left and right ordinates apply respectively to the blue and pink lines. (From ref.⁸).

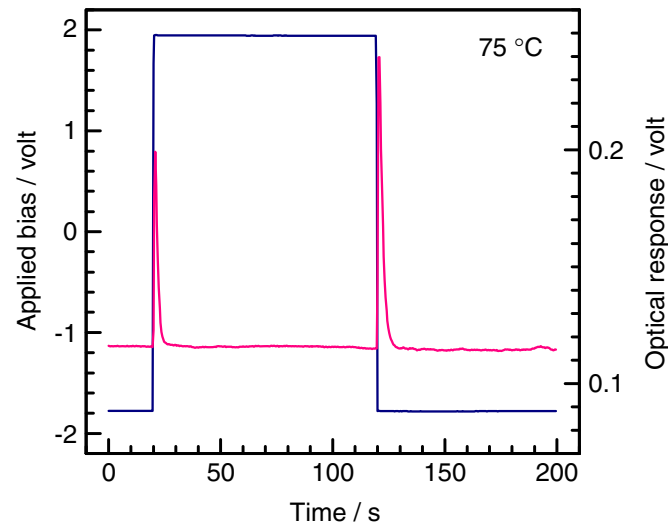
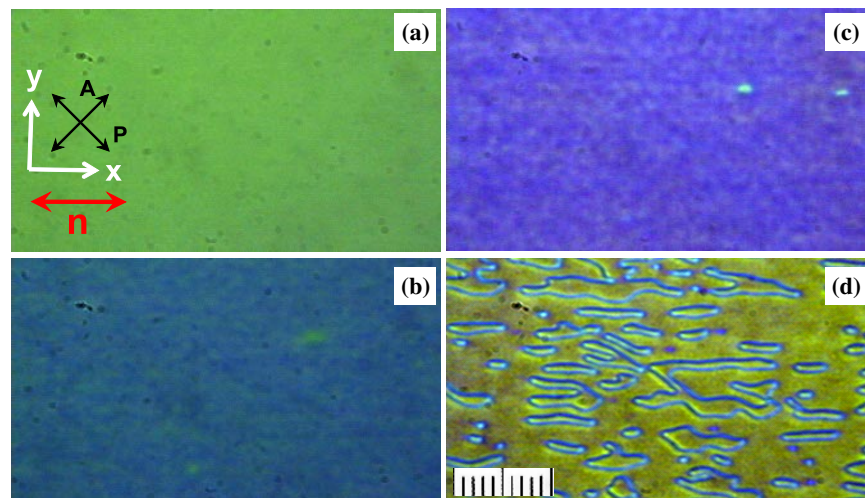


Figure 9: Interference colours in a $7.75 \mu\text{m}$ thick sample; diagonally crossed polarizers, P(45)-A(135); unfiltered mercury light. Applied bias: (a) 0 V, (b) 2.04 V, (c) 3.07 V and (d) 4.11 V. $10 \mu\text{m}/\text{scale}$ division. $75 \text{ }^\circ\text{C}$. (From ref.⁸).



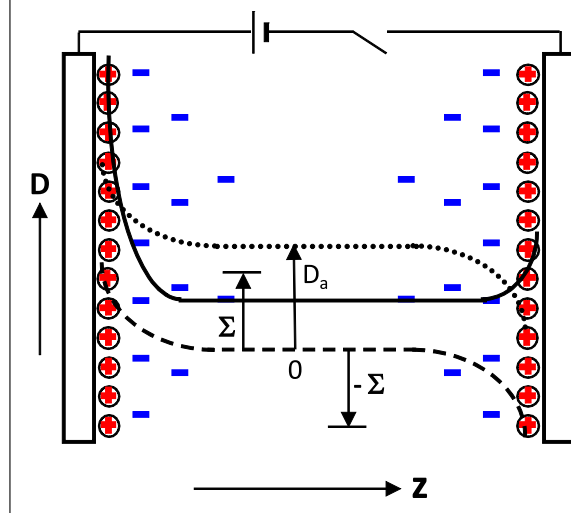
An alternative interpretation of the homogeneous distortion at low voltages is to consider it as due to the coupling between the GF and BP instabilities^{17b}; in this case, the BP threshold V_f decreases to V_{fr} and the period of the longitudinal domains Λ increases to Λ_m :

$$V_{fr} = \frac{V_f}{1+\nu} \left(1 - \frac{V_f}{4V_G} \right);$$

$$\Lambda_m = d \sqrt{\frac{1+\nu}{1-\nu - \left(\frac{V_f}{2V_G} \right)}}$$

Here $\nu = \epsilon_o \epsilon_a k_i / e^2$, with $e = (e_S - e_B)$. In particular, for $2V_G \leq V_f / (1 - \nu)$, the periodicity of the pattern vanishes. From earlier measurements⁸, at 55°C , $k_i = 9.6 \text{ pN}$, $e = 5.95 \text{ pCm}^{-1}$, $V_f = 6.4 \text{ V}$ and $\epsilon_a = 0.21$; thus, $V_f / [2(1 - \nu)] \approx 6.4 \text{ V}$; when

Figure 10: Schematic of the displacement (D) field in the sample at various times en route equilibrium. Σ denotes the surface charge density of adsorbed positive ions at the electrodes. The D -field is represented by the dashed curve in the absence of bias, dotted curve immediately after applying a bias corresponding to D_a , and continuous curve in the equilibrium state. (From ref.⁸).



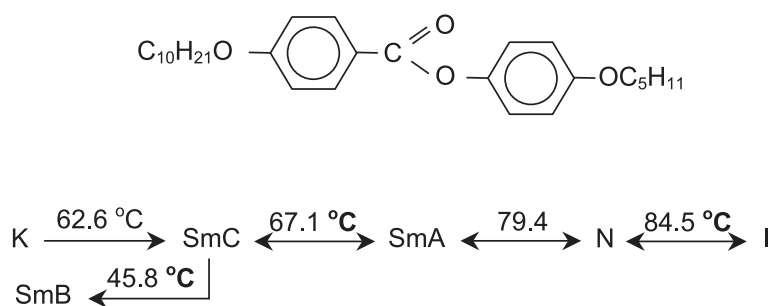
V_G is below this value, the distortion is predicted to become homogeneous.

A linear field variation across the sample, such as supposed in the above discussion, would imply a constant density of injected charges. This condition is generally difficult to fulfill in usual nematics acting as weak electrolytes. The equilibrium field distribution in a nematic under a dc voltage is often complex; the field, while remaining homogeneous in bulk, will rapidly increase toward the electrodes within the Debye-like screening layers due to the formation of counterion layers adjacent to the electrodes¹⁹. Charge injection that may occur when no blocking layers are present, will render the surface field asymmetric while leaving the bulk field uniform²⁰. The bulk field uniformity is undisturbed even when blocking layers are used; with selective adsorption of ions of the same sign at these layers, however, the surface field asymmetry becomes permanent; differential mobility of the oppositely charged ions results in a similar field configuration, except for the surface field asymmetry which is now transient²¹. These ideas are quantitatively explored in a recent analysis of the influence of ions on the dynamical response of a nematic subject to a static field²².

Significantly, we observe the GF switching in BEPC even when the electrodes are coated with blocking layers of polyimide. Therefore charge injection cannot be the sole reason for field inhomogeneity in bulk. As mentioned above, the equilibrium field gradients set up by segregated counterions are confined to thin boundary layers

and are unlikely to give rise to detectable GF distortions. The transient director switch probably involves two counter contributory, time-dependent factors that prevail on the route to equilibrium: First, with efflux of time, the regions on either side of the midplane $z = 0$, wherein the displacement gradient dD/dz is nonzero, shrink gradually toward contiguous electrodes. Second, dD/dz increases simultaneously in these regions. This dynamic situation is quite possible under selective ion adsorption at the electrodes, such as discussed by Thurston²³. For the sake of argument, consider positive ions as adsorbed resulting in a surface charge density, $+\Sigma$ (Figure 10). In the absence of external field, diffuse negative ion layers form opposite these immobile positive ions. The resulting intrinsic double layer field, previously analyzed in detail²¹, would be as shown by the dashed curve. Soon after applying a dc field corresponding to a displacement D_a , the initial field gets shifted by D_a to the position indicated by the dotted curve. With passage of time, the diffuse negative layer next to the cathode is drawn toward the anode, while the mobile positive ions drift toward the cathode. Eventually, the equilibrium configuration shown by the continuous curve is attained. The charging process in itself takes a very short time, a fraction of a millisecond. But the time τ_d taken by the charges to drift across the cell may be of the order of seconds. For example, from $\tau_d = d^2/(\mu V)$, μ being the mobility ($\sim 10^{-11} \text{ m}^2/\text{Vs}$) and d ($= 8 \text{ }\mu\text{m}$) the thickness of the sample subject to 1.5 V, τ_d is $\sim 4 \text{ s}$. During this time, while the transition between the

Diagram 1:



states represented by the dotted and continuous curves occurs, field gradients that induce a transient GF reorientation could exist in bulk. When charge injection is also present, the switching effect may be prolonged and amplified.

4. Travelling undulations in an achiral smectic C liquid crystal excited by a static electric field

4.1. Propagative phenomena

In liquid crystals, electric field driven propagative phenomena arise for a variety of reasons. Quite often, the instability is short-lived, occurring only while an energetically more favourable director configuration grows at the expense of a less favourable one. Some examples of such a transient effect are: The collapse of an annular Brochard-Leger (BL) wall between two degenerate Freedericksz states of a nematic²⁴; drift of domain walls in achiral smectic C (SmC) liquid crystals well above the Freedericksz threshold²⁵; and moving wall fronts in the SmC* phase under a dc field²⁶. Sustained propagation not limited by finite size effects is relatively less common. A well-known example of it is the Hopf bifurcation into the travelling roll electroconvective state in nematic liquid crystals; it is explained by the weak electrolyte model based on the presence of two mobile ionic species in the fluid [27]. We have observed [9] a different type of sustained, static-field-driven propagative phenomenon associated with the undulations of SmC layers, which appears to result from a coupling between the transverse field gradients and transverse component of flexoelectric polarization. In this Section, we describe the characteristics of this instability and discuss its possible origin.

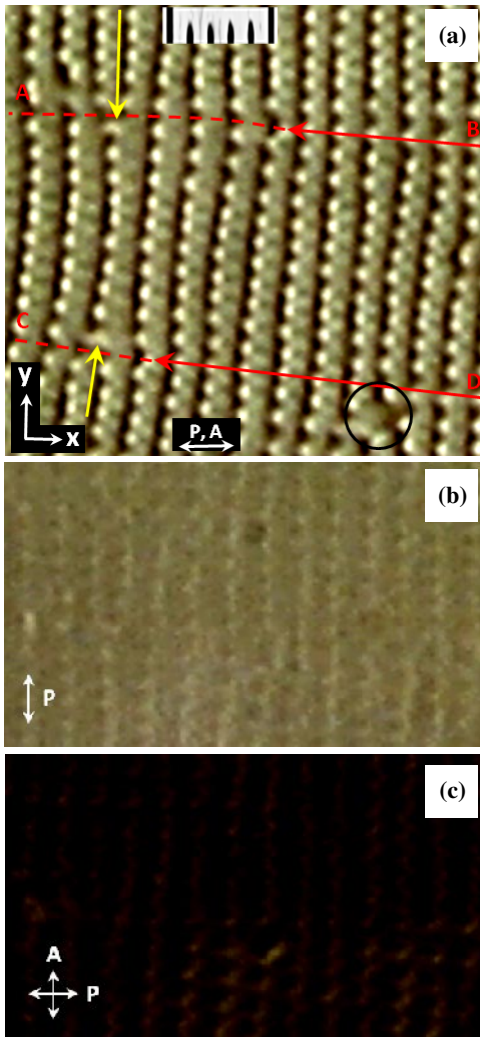
4.2. Undulatory instability in the smectic C phase of a phenyl benzoate

The compound used in this study is 4-n-pentyloxyphenyl 4-n-decyloxybenzoate (POPDOB) with the structure and phase sequence given in see Diagram 1.

Experimental details are given in⁹. Briefly, a thin film of the material ($d \sim 30 \mu\text{m}$), held between unidirectionally buffed conducting glass plates is studied in transmitted light, along z , the layer normal, using a polarizing microscope. The electric field acts along $\pm z$. The sample shows a planar alignment on cooling to the nematic phase, near the clearing point. But, a few degrees below, at $\sim 80^\circ\text{C}$, an anchoring transition to the homeotropic state takes place. In the SmA state, this alignment is maintained. Upon further cooling into the SmC state, the layers develop an undulatory instability. Well inside the SmC phase, the undulations are two dimensional (2-D), with the wave vectors mostly along x , the rubbing direction, and y , the C₂ rotation axis of the structure. The corresponding optical texture exhibits a two dimensional array of focal images as in Figure 11a. Seen through a polarizer P, the texture appears with maximum contrast for P(0), i.e., for the transmission axis along x (Figure 11a); the contrast is minimum for P(90) (Figure 11b); and, between crossed polarizers P(0)–A(90), the field of view is nearly dark (Figure 11c). These observations reveal that, within the undulatory layers, the c -director is predominantly along x so that the extraordinary vibration along x experiences a periodic modulation of the index.

Johnson and Saupé²⁸ have made a detailed analysis of the layer undulation instability which is thermally excited in the SmC state. The structural differences between the SmA and SmC phases are believed to be responsible for this instability. In²⁸, the substrates were silane treated; this led, during cooling from the isotropic phase, to the formation of homeotropic nematic and SmA textures; on passing into the SmC, the texture displayed schlierens and, upon further cooling, undulation lines appeared radially and tangentially around the line singularities. The undulations are interpreted as due to the tilting of the director away from the layer normal; consequent on the tilt increase with cooling, the layers tend to contract increasingly more, but the spacers determining the thickness contract less. The resulting mechanical stress, in the absence of nucleation of new layers, leads to the undulations. With our samples, the unidirectional buffing of the substrates lifts the tilt degeneracy to provide a monostable domain with the c -director along x . Otherwise, the undulations in POPDOB possess similar structural characteristics as those reported in²⁸.

Figure 11: Two-dimensional array of focal images due to the undulations with wave vectors predominantly along x and y in a smectic C film of POPDOB at 58 °C. Polarizer P and analyzer A are oriented as indicated by double-headed arrows. In (a), red and yellow arrows indicate edge dislocations and the black circle a vacancy in the lattice; 2 μm per scale division. (From ref.⁹).



4.3. Phase propagation within the undulatory structure

When a sample of POPDOB in the SmC phase with the 2-D undulatory structure is exposed to a gradually increasing dc field, travelling wave (TW) instability develops above a threshold that varies from region to region. In other words, the TW phenomenon is localized and occurs at different thresholds in different sample zones. Further, it is associated only with the undulations corresponding to the wave vector \mathbf{q}_x and no TW instability is seen along the wave vector \mathbf{q}_y . Optically, the onset of instability manifests as a continual drift of the columns of focal images along x , as depicted in

Figure 12. That the observed effect is caused by phase fluctuations rather than fluid motion is borne out by the absence of any coordinated dust particle motion in the fluid. Presumably structural defects play an important role in localization of the TWs. Apparently, the defects tend to impede and arrest the propagation; in fact, different localized zones of instability are found to be demarcated by defect ridden horizontal bands. For instance, in Figure 11a, a propagation zone is found between the lines AB and CD along which edge-like dislocations are situated; the dislocations corresponding to the wave vector \mathbf{q}_y emerge at positions indicated by the red arrows; and those of opposite sign and corresponding to \mathbf{q}_x , are located at positions indicated by the yellow arrows.

With a progressive increase in applied bias, the TW-zones become more and more numerous and, at a high enough voltage, the instability is observed in the entire sample. An interesting aspect of the TW phenomenon is the nonuniformity of drift speed. It is readily noticed near the threshold as unsteady motion of the columns of focal spots; these focal arrays move swiftly between their equilibrium positions and become momentarily stationary each time they are in register. This hopping character of TWs gets blurred on raising the control parameter or increasing the propagation speed v_p . Here, as in nematic electroconvection (NEC), we take the control parameter, ε , to be defined by $\varepsilon = (V^2 - V_{th}^2)/V_{th}^2$, where V and V_{th} are the applied and threshold voltages, respectively. Figure 13 presents the dependence of v_p on ε ; v_p increases nearly linearly upto $\varepsilon \approx 2$; it tends to saturate thereafter presumably because of the increase in defect density at higher fields. Significantly, v_p approaches zero along with ε . By contrast, the traveling waves in NEC possess a nonzero threshold speed nearly the same as that of convective motion inside a roll²⁹. The drifting undulations are a different phenomenon compared to the TWs in NEC and we observe no convective flows in the SmC phase here.

As previously indicated, a given voltage generally corresponds to different values of ε in different regions; that is, V remaining constant, v_p varies from region to region. Conceivably, v_p is determined by various factors such as the number and nature of defects in the demarcating bands, substrate irregularities due to rubbing and foreign impurities disrupting the lattice. The most decisive feature of the TW instability, as far as its origin is concerned, is the reversal of drift direction with every reversal of field polarity. For a fixed voltage, most often, the forward and reverse drifts occur at very different speeds in any given drift-zone. This is again related to widely differing ε -values, or thresholds, for the

Figure 12: Snapshots of travelling undulations at 90 V, 58 °C with the polarizers along x ; (b) is captured a fraction of a second after (a). Slanting arrows indicate the corresponding columnar arrays. Horizontal dimension is 27 μm . (From ref.⁹).

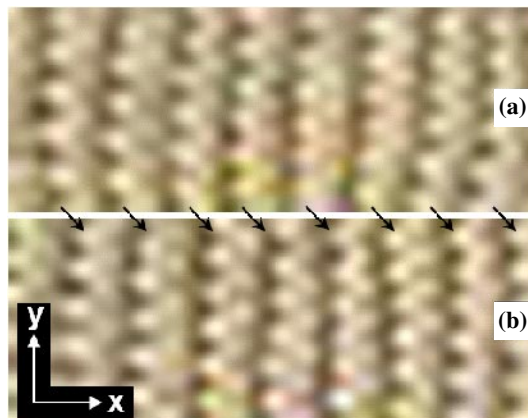
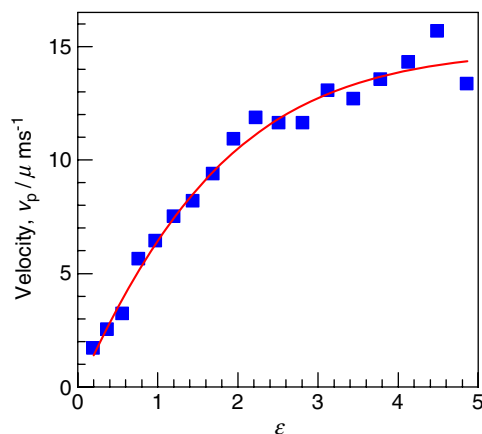


Figure 13: Propagation velocity v_p as a function of the control parameter $\varepsilon = (V^2 - V_{th}^2)/V_{th}^2$, V and V_{th} denoting the applied and threshold voltages respectively. $V_{th} = 64$ V. 58 °C. (From ref.⁹).



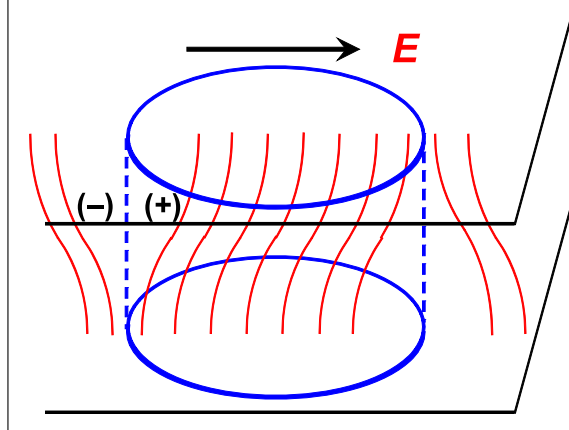
forward and reverse drifts in a given region. Under a very low frequency high voltage square wave field, the switching of the drift direction with the field is clearly observed. The TW state is not obtained above a few Hz when this oscillatory motion stops altogether.

4.4. Qualitative interpretation of the TW phenomenon

The mechanism causing the propagative instability probably involves a coupling between different electrical responses. To simplify our discussion of this interaction, we may suppose the SmC phase to be uniaxial rather than biaxial. An obvious source of destabilization is the dielectric anisotropy ε_a

which is nearly a constant (≈ -0.8) in the SmC phase of POPDOB³⁰. When ε_a is negative, a SmA-like homeotropic film, strongly anchored at the substrates and submitted to an electric field along its optical axis, may develop the Helfrich-Haurault^{31,32} type of undulatory distortion of the layers, which, in general, may be two-dimensional³⁴⁻³⁶. If the layers are initially undulated and the local displacement $u(x, y, z)$ is given in terms of the maximum amplitude u_0 and d by $u(x, y, z) = u_0 \sin(q_x x) \sin(q_y y) \sin(\pi z/d)$, the field may so enhance u_0 as to maximize the director component transverse to it. Further, it may render the undulation profile nonsinusoidal by inducing higher Fourier modes. When the anchoring at the substrates is soft,

Figure 14: Schematic of an elliptical wall in an initially homeotropic nematic, with a positive dielectric anisotropy, acted upon by an in-layer electric field E . Splay bend distortions occur along the principal axis parallel to E and twist bend distortions, along the other principal axis. (–) and (+) are the tilt signs.



under a strong field, the instability may tend toward ‘buckling’ in which the z dependence of the curvature gets weakened³⁶. The dielectric destabilization may also generate a Freedericksz-like reorientation without affecting the layer distortion⁹. In any event, the dielectric effects are quadratic in field and cannot account for the drift instability that is field direction dependent.

The TW state in POPDOB is in all likelihood a result of the inverse flexoelectric response. It is known that an undistorted SmC layer, when acted on by an electric field in the tilt plane (\mathbf{k} , \mathbf{c}), \mathbf{k} being the layer normal and \mathbf{c} the local tilt direction, may display five distinct flexo-distortion modes, each described by two independent vector fields and corresponding flexocoefficients³⁷. Two of these modes are also found in the 2-D undulatory structure (Figure 11); in each flexo-mode, while one of the two fields creates a dipole density along \mathbf{c} , the other creates it along \mathbf{k} . However, in the absence of electric field, provided the undulations are of sine wave symmetry, no net flexopolarization exists. A dc field along z may be expected to break the up-down symmetry of the wave form generating a net flexopolarization along the field direction.

How does the flexopolarization destabilize the \mathbf{q}_x undulations? While speculating on this question, it is necessary to recall that the coupling between layer bending and conductivity anisotropy σ_a could give rise to the Carr-Helfrich³⁸ type periodic charge focusing. Thus transverse fields may develop along x for the \mathbf{q}_x -undulations. Since the smectic structure does not support material transport across the layers, not surprisingly, we found no electroconvective flows despite the possible space charge creation. However, the periodically varying transverse field

E_x could destabilize the structure in a different way: In SmC undulations, because of the director tilt with respect to the layer normal, a net polarization along x could be expected. The coupling between this polarization and the spatially varying transverse field E_x would lead to a net drift force along x . On reversal of the field, the drift force also changes sign. When the undulations become nonsinusoidal as a result of dielectric and flexoelectric reorientations as earlier noted, the drift effect may become more pronounced. The loss of rotational symmetry within the SmC layers may further contribute to the reduced symmetry of the undulation profile. These considerations also account for the absence of propagation for the \mathbf{q}_y -undulations since, along y , no significant flexopolarization is expected.

5. Asymmetric deformation of annular walls in free-standing nematic films subject to inplane electric fields

5.1. Leger–Brochard walls

The electric Freedericksz effect in nematic liquid crystals is studied mostly in the sandwich geometry, employing planar or homeotropic samples with the field along the layer normal³⁹. Above a voltage threshold, the director reorients such that the tilt decreases from its maximum value in the midplane to zero at either substrate. Since nematics are apolar, the positive and negative tilts, which are equivalent in free energy, tend to occur with equal probability. Adjacent regions of opposite tilt are bridged by a wall, often referred to as the Brochard–Leger (BL) wall^{40–42}. We are concerned here with closed BL walls of the type in Figure 14. The properties of such walls formed in the course of magnetic Freedericksz reorientation have been

Figure 15: (a) Sample geometry showing the electrodes S, insulating bridges B, $-1/2$ disclination loop L, and axes of reference (x, y, z) . (b) A possible director pattern given by the dotted lines with the disclinations at opposite electrodes situate on either side of the mid $z=0$ plane. (c) Interference fringes near the electrodes observed in PCH5, in the field-free state, using mercury green light and diagonally crossed polarizers. The central dark zone is homeotropic. (From ref.¹⁰).

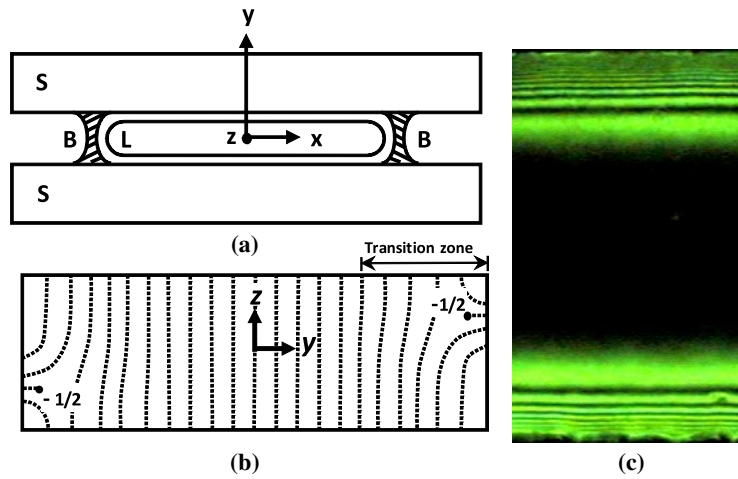
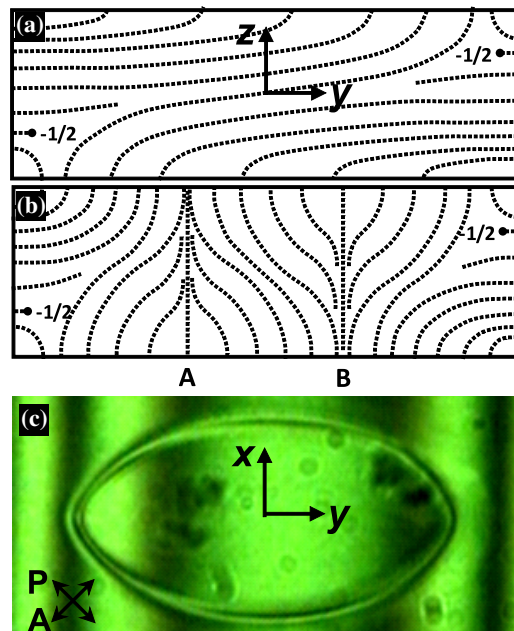


Figure 16: (a) The director pattern (dotted lines) well above threshold depicting the merger of the transition layers from opposite electrodes. (b) Director field showing the formation of an annular wall in the course of dielectric reorientation on sudden application of the field. (c) A nearly elliptical wall observed in a $75 \mu\text{m}$ thick film of PCH5; $f = 25 \text{ kHz}$, $V = 50 \text{ V}$, $\Gamma = 325 \mu\text{m}$. (From ref.¹⁰).



theoretically analyzed⁴⁰. First, closed walls are metastable and spontaneously collapse to minimize energy. Second, their equilibrium geometry is an ellipse such that the ratio of semi major to semi minor axis (a/b) is related to the ratio of elastic

moduli as $a/b = (k_{11}/k_{22})^{1/2}$, where $i = 1$ or 3 depending on whether the initial alignment is homeotropic or planar. These and other predictions relating to the dynamics of closed walls have been verified by Leger⁴¹ in her magnetic field experiments.

Figure 17: Shear distortion in a cylindrical wall exposing the sides facing the electrodes and defect lines in the SB regions. Unfiltered mercury light; diagonally crossed polarizers; $f = 25$ Hz, $V = 50$ V, $d = \mu\text{m}$, $\Gamma = 360 \mu\text{m}$. (From ref.¹⁰).

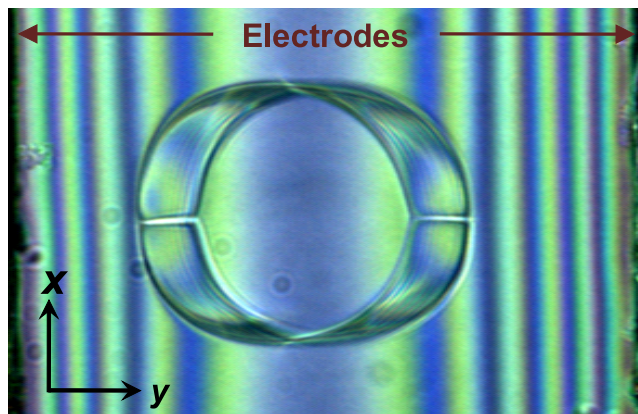
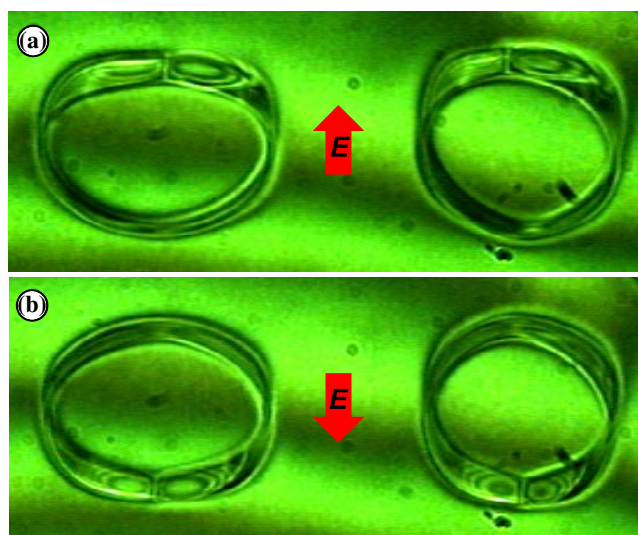


Figure 18: Effect of field reversal on distortion in the SB regions; 0.2 Hz square wave field, 40 V; $d = 113 \mu\text{m}$, $\Gamma = 435 \mu\text{m}$; mercury green light, diagonally crossed polarizers; (a) and (b) are the interferograms of collapsing loop walls captured at an interval of a few seconds with the indicated field directions. (From ref.¹⁰).



Electrically induced walls are more complex⁴³ compared to magnetically induced walls because of ionic impurities⁴¹. In some recent investigations on electrically excited closed walls in freely suspended films under an inplane field^{10,44}, several new features involving electrical conduction have come to light. Important among these are (i) shearing of loop-walls revealing discontinuity of the wall along the field direction, in the splay-bend (SB) region, (ii) dependence of the wall-ellipticity on field frequency, (iii) multiple division of walls under high field

strengths and (iv) asymmetrical deformation at the opposite SB regions under a dc bias, attributable to flexoelectric polarization. We focus here on the last of these aspects.

5.2. Flexo-influence on shear strained cylindrical walls in a nematic

Consider a nematic having a strong terminal polar group resulting in a large positive ϵ_a ; for specificity, we take 4-(*trans*-4'-pentylcyclohexyl) benzonitrile (PCH5). Figure 15a shows a thin film

of it, held between two metal strips spaced Γ apart. Instabilities are studied using a field $E = V/\Gamma$, acting along y , transverse to the observation direction z . The sample usually aligns spontaneously in a way that the director is normal to *all* the limiting surfaces so that a $-1/2$ disclination loop forms peripherally (Figure 15b). For P(45)-A(135), the splay-bend transition regions formed next to the electrodes produce parallel birefringence fringes as in Figure 15c. A possible field-free state director configuration accounting for the fringes and of interest in further discussion here is shown in Figure 15b. Under a gradually increasing field, the transition layers begin to expand toward the midregion at a threshold slightly lower than the Freedericksz threshold $E_F = \frac{V_F}{\Gamma} = \left(\frac{\pi}{d}\right) \sqrt{\frac{k_{33}}{\epsilon_0 \epsilon_a}}$ that applies to a completely homeotropic film with no lateral boundary effects. Eventually, for the initial director pattern as in Figure 15b, the layers merge so that the alignment is essentially planar away from the boundaries (Figure 16a). However, if a field slightly above E_F is suddenly applied, simultaneously with the transition zones beginning to grow, reorientation also occurs in the midregion; under these conditions, closed walls may form as schematically shown in Figure 16b; Figure 16c presents a nearly elliptical wall observed using a high frequency (25 kHz) field.

Under a low frequency (25–150 Hz), high intensity ($\sim 4E_F$) field, a remarkable new instability is exhibited by the annular walls in free-standing films, the like of which is not encountered in sandwich geometry. It consists of the shearing of the top and bottom free-surfaces of the domain enclosed by the wall. In Figure 17 we present a typical shear-distorted cylindrical wall in which the opposite sides facing the electrodes have become visible. Most interestingly, in the SB regions at the extremities of the principal axis along y , structural discontinuities appear. The shear is basically produced through Carr-Helfrich mechanism based accumulation of opposite charges on the free surfaces of the cylindrical domain and the structural discontinuities are the Neel-like lines between oppositely twisted regions¹⁰.

The shear sense is not polarity dependent. Under ac excitation, with every field reversal, the charges on the two domain faces interchange to produce a steady strain of the annular walls. However, when a very low frequency square wave field is employed to induce the shear strain, another novel, polarity-sensitive feature of distortion is revealed. We describe this with reference to Figure 18 showing two annular walls; both the walls in Panel 18a are clearly exhibiting a greater degree of distortion in the upper SB region compared to the lower region;

in Panel 18b corresponding to a reversed field, the deformation asymmetry is quite the opposite. All through the domain collapse, the distortion asymmetry keeps reversing between the two SB regions at double the frequency of the field. We may ascribe this effect to flexopolarization \mathbf{P}_f associated with the SB regions. In an unsheared elliptical wall, the opposite SB deformations are related by inversion symmetry. Accordingly, in the two regions, \mathbf{P}_f is oppositely directed, with the up-down disposition, so that no net effect is obtained; In a sheared annular wall, the SB parts are tilted and \mathbf{P}_f acquires an inplane component \mathbf{P}_{fy} ; but this component is directed oppositely in the two regions so that there is no net effect again as long as the extents of distortion in these regions do not differ. Since a net \mathbf{P}_{fy} along \mathbf{E} lowers the free energy, it is reasonable to suppose that the SB distortion becomes stronger where the inplane polarization is along \mathbf{E} , relative to the other region where it is opposite.

6. Concluding remarks

Flexoelectricity is a universal property of liquid crystals that may produce reorientational effects by itself; it may also have a widespread influence on various other electric field driven phenomena. We have provided here a few examples of the converse flexoeffect that demonstrate both these aspects: The first is seen in flexoelectrooptic switching at defect sites and gradient flexo-switching at polarity reversals; and the second, in the TW instability in the SmC phase and asymmetric deformation in sheared loop-walls, both of which seem to involve Freedericksz, Carr-Helfrich and flexoelectric mechanisms of destabilization. The interpretation of these less known effects has been qualitative, serving to indicate the importance of flexopolarization in electric field experiments. Obviously, these effects need further exploration for a better understanding; and, in particular, the remarkable phenomenon of phase propagation in undulatory structures merits a closer examination and theoretical analysis.

Acknowledgements

We thank Professor K. A. Suresh for his support and encouragement. K.S.K. is thankful to the Department of Science and Technology, India for the Indo-Bulgarian research project under which part of the work reviewed here was conducted.

Received 18 February 2009.

References

1. R. B. Meyer, *Phys. Rev. Lett.* 1969, 22, 918.
2. P. Rudquist, S. T. Lagerwall, *Liq. Cryst.* 1997, 23, 503.

3. (a) J. Harden, B. Mbanga, N. Eber, K. F.-. Csorba, S. Sprunt, J. T. Gleeson, A. Jakli, *Phys. Rev. Lett.* 2006, 97, 157802; (b) J. Harden, R. Teeling, J. T. Gleeson, S. Sprunt, and A. Jakli, *Phys. Rev. E* 2008, 78, 031702.
4. J. Prost, J. P. Marcerou, *J. Phys. Fr.* 1977, 38, 315.
5. (a) J. C. Jones, *SID Digest XXXVII, Book II* 2006, 51.2, 1626 and references therein ; (b) S. Kitson, A. Geisow, *Appl. Phys. Lett.* 2002, 80, 3635.
6. (a) N. V. Madhusudana, V. A. Raghunathan, *Liq. Cryst.* 1989, 5, 1789; (b) L. Kramer, E. Bodenschatz, W. Pesch, W. Thom, W. Zimmermann, *Liq. Cryst.* 1989, 5, 699; (c) A. Krekhov, W. Pesch, N. Eber, T. T.- Katona, A. Buka, *Phys. Rev. E* 2008, 77, 021705; (d) T. T.- Katona, N. Eber, A. Buka, A. Krekhov, *Phys. Rev. E* 2008, 78, 036306.
7. P. Kumar, K. S. Krishnamurthy, *Liq. Cryst.* 2006, 33, 131.
8. P. Kumar, K. S. Krishnamurthy, *Liq. Cryst.* 2007, 34, 257.
9. K. S. Krishnamurthy, P. Kumar, *J. Phys. Chem. B* 2007, 111, 2423.
10. P. Tadapatri, K. S. Krishnamurthy, *J. Phys. Chem. B* 2008, 112, 13509.
11. J. Nehring, A. Sauepe. *J. Chem. Soc. Faraday trans. II*, 1972, 68, 1.
12. M. Kleman, C. Williams, *Phil. Mag.* 1973, 28, 725.
13. P. Rudquist, E. Korblova, D. M. Walba, R. Shao, N. A. Clark, J. E. Maclennan. *Liq. Cryst.* 1999, 26, 1555.
14. J. S. Patel, R. B. Meyer. *Phys. Rev. Lett.* 1987, 58, 1538.
15. A. G. Petrov, *Physical Properties of Liquid Crystals: nematics*, D. A. Dunmur, A. Fukuda, G. R. Luckhurst (Eds), INSPEC-IEE, London, 2001.
16. S. A. Pikin, *Structural Transformations in Liquid Crystals*, Gordon and Breach Science Publishers, New York, 1991.
17. (a) A. I. Derzhanski, A. G. Petrov, H. P. Hinov, B. L. Markovski, *Bulg. J. Phys.* 1974, 1, 165. (b) A. Derzhanski, A. G. petrov, *Advances in Liquid Crystal Research and Applications*, Vol. 1, L. Bata (Ed), Pergamon Press, Oxford, 1980. (c) A. I. Derzhanski, A. G. Petrov, *Acta Phys. Pol.* 1979, A55, 747.
18. (a) Y. P. Bobylev, V. G. Chigrinov, S. A. Pikin, *J. Phys. (Paris)*, 1979, 40 (suppl. 4), C3- 331. (b) Y. P. Bobylev, S. A. Pikin, *Sov. Phys. JETP*, 1977, 45, 195.
19. G. Barbero, D. Olivero, N. Scaramuzza, G. Strangi, C. Versace, *Phys. Rev. E* 2004, 69, 021713.
20. Sun Lu, D. Jones, *Appl. Phys. Lett.* 1970, 16, 484 (1970).
21. R. N. Thurston, J. Cheng, R. B. Meyer, G. D. Boyd, *J. Appl. Phys.* 1984, 56, 263.
22. M. Scalerandi, P. Pagliusi, G. Cipparrone, G. Barbero, *Phys. Rev. E* 2004, 69, 051708.
23. R. N. Thurston, *J. Appl. Phys.* 1984, 55, 4154.
24. (a) F. Brochard, *J. Phys. (Paris)* 1972, 33, 607. (b) L. Leger, *Mol. Cryst. Liq. Cryst.* 1973, 24, 45. (c) K. S. Krishnamurthy, M. S. Bhate, *Mol. Cryst. Liq. Cryst.* 1985, 128, 29.
25. (a) P. Schiller, G. Pelzl, D. Demus, D. *Liq. Cryst.* 1987, 2, 21 and 131. (b) I. W. Stewart, T. Carlsson, F. M. Leslie, *Phys. Rev. E* 1994, 49, 2130.
26. P. E. Cladis, W. van Sarloos, Some nonlinear problems in anisotropic systems. In *Solitons in Liquid Crystals*; I. Lam, J. Prost, Eds.; Springer-Verlag, New York, 1992; Ch. 4, pp 110–150.
27. M. Dennin, M. Treiber, L. Kramer, G. Ahlers, D. S. Cannell, *Phys. Rev. Lett.* 1996, 76, 319.
28. D. Johnson, A. Sauepe, *Phys. Rev. A* 1977, 15, 2079.
29. A. Joets, R. Ribotta, *Phys. Rev. Lett.* 1988, 60, 2164.
30. H. Kresse, A. Wiegeleben, D. Demus, *Krist. Tech.* 1980, 15, 341.
31. (a) W. Helfrich, *Appl. Phys. Lett.* 1970, 17, 531; (b) J. P. Hurault, *J. Chem. Phys.* 1973, 59, 2086.
32. S. Chandrasekhar, *Liquid Crystals*, 2nd ed; Cambridge University Press: Cambridge, 1992; pp 313–316.
33. H. Pleiner, R. Stannarius, W. Zimmerman, Electrically driven instabilities in smectic liquid crystal films. In *Evolution of Structures in Continuous Dissipative Systems*; F. Busse, S. C. Muller, Eds.; Springer, Berlin, 1998; pp 285–324.
34. S. Ried, H. Pleiner, W. Zimmermann, *Europhys. Lett.* 2000, 52, 525.
35. I. W. Stewart, *Liq. Cryst.* 2003, 30, 909.
36. B. I. Senyuk, I. I. Smalyukh, O. D. Lavrentovich, *Phys. Rev. E* 2006, 74, 011712.
37. S. T. Lagerwall, *Ferroelectric and Antiferroelectric Liquid Crystals*; Wiley-VCH: Weinheim, 1999; Ch. 4, pp 107–114.
38. W. Helfrich, *J. Chem. Phys.* 1969, 51, 4092.
39. L. M. Blinov, V. G. Chigrinov, *Electrooptic Effects in Liquid Crystal Materials*; Springer: Berlin, 1994.
40. F. Brochard, *J. Phys. (Paris)* 1972, 33, 607.
41. L. Leger, *Mol. Cryst. Liq. Cryst.* 1973, 24, 33.
42. X. Y. Wang, *Phys. Lett.* 1985, 112A, 402.
43. K. S. Krishnamurthy, M. S. Bhate, *Mol. Cryst. Liq. Cryst.* 1985, 128, 29.
44. K. S. Krishnamurthy, R. Balakrishnan, *Pramana* 2003, 61, 263.



Professor K. S. Krishnamurthy is an Emeritus Scientist at the Centre for Liquid Crystal Research, Bangalore. He received his Ph. D. from the University of Mysore in 1971. He joined the Defence Research and Development Organization soon after, and was posted to the College of Military Engineering, Pune where he was the Professor of Applied Sciences from 1989 till his retirement in 2004. His current research interests concern dielectric, flexoelectric and electrohydrodynamic effects in liquid crystals.



Pramoda Kumar is a CSIR Senior Research Fellow, carrying out doctoral studies on "Field Driven Reorientational and Convective Instabilities in Nematic Liquid Crystals" at the Centre for Liquid Crystal Research, Bangalore. He received his Master of Science degree in Physics from Mangalore University in 2001.



Pramod Tadapatri, a DST Junior Research Fellow at the Centre for Liquid Crystal Research, Bangalore, is engaged in doctoral studies on "electric-field generated instabilities in thermotropic liquid crystals". He received his Master of Science degree in Physics from Mysore University in 2007.